

DESIGN OPTIMISATION OF AN UNMANNED UNDERWATER VEHICLE

FIRDAUS ABDULLAH^{1*}, MATTHIEU FERRARO², ANDREW RIGIT³

¹Dept. of Design & Tech., Loughborough University, LE11 3TU Leicestershire, UK

²Dept. of Mech. Eng., University of Technology of Belfort-Montbéliard, FRANCE

³Faculty of Engineering, University of Sarawak, MALAYSIA

* Corresponding Author: m.f.a.abdullah@lboro.ac.uk

Abstract

The results of fluid flow simulation around an unmanned underwater vehicle (UUV) are presented in this paper. The UUV represents a small submarine for underwater search and rescue operation, which suits the local river conditions. The flow simulation was performed with a commercially available computational fluid dynamics package, Star-CD. The effects of the UUV geometry on the velocity and pressure distributions on the UUV surface were discussed for $Re = 500,000$ and $3,000,000$. The discussion led to an improved design of the UUV with a smoother velocity profile around the UUV body.

Keywords: CFD, UUV, Design Optimisation.

1. Introduction

An unmanned underwater vehicle (UUV) is a small submarine, which normally being deployed for various dangerous underwater tasks that include search and rescue operation. UUVs are very useful in executing and completing dangerous task effectively with minimum cost and risks [1]. It is desirable to have a smoother as possible velocity profile around a UUV body in order to obtain a better stability and control of the small submarine [2]. It is therefore important to know the effects of fluid flow conditions around a UUV when it is submerged in a river during a typical search and rescue operation. Therefore, the main objective of this paper is to present the fluid flow visualization around a UUV. The results will help to decide how the shape of the UUV can be modified in order to obtain a uniform velocity profile around the UUV.

Nomenclatures

g_m	Gravitational field component
\sqrt{g}	Determinant of metric tensor
p	Piezometric pressure
p_s	Static pressure
s_i	Momentum source components
s_{ij}	Rate of strain tensor
s_m	Mass source
t	Time
u'	Fluctuation about the ensemble average velocity
u_i	Absolute fluid velocity component
u_j	Relative velocity between fluid and local (moving) coordinates

Greek Symbols

δ_{ij}	Kronecker delta = 1 when $i = j$ and zero if otherwise
ρ	Density
τ_{ij}	Stress tensor
μ	Molecular dynamic fluid viscosity

2. Computational Modelling

2.1 The UUV models evaluated

Two UUV models were studied in this paper and a 3-D drawing of the two were shown in Figs. 1 and 2 respectively. Fig. 1 represents a UUV model with a hole at each of its side whilst Fig. 2 shows a UUV model without a hole.

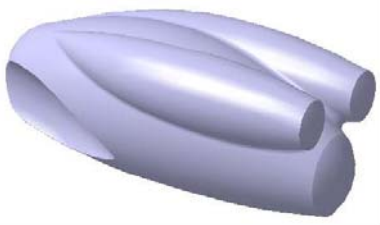


Fig. 1. A 3-D Drawing of A UUV Design with Holes.

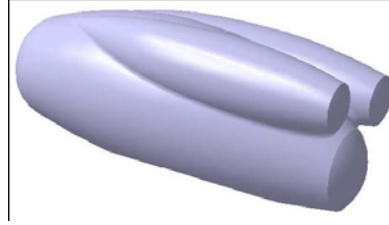


Fig. 2. A 3-D Drawing of A UUV Design without Holes.

2.2 The CFD model

The flow predictions were carried out using a commercially available CFD package, Star-CD. The solid geometry of the model, modelled using Catia, was then exported into ProStar [3] of Star-CD. The meshing of the model was done manually and the steps involved were [3] to:

1. create vertex points or vertices on the model,
2. create blocks based on the vertices,
3. map meshing onto the surfaces, and
4. cell-meshing created and refined based on model requirement.

A high-quality grid leads to an accurate CFD solution. Therefore, the grid refinement was made properly and the grid was realized with tetrahedral cells as shown in Figs. 3 and 4. The first model has 1,111,040 tetrahedral fluids-cells and 33,182 partials boundaries (Fig. 3). The submarine second model has 632,309 tetrahedral fluids-cells and 30,220 partials boundaries (Fig. 4). The high number of cells for the first model was due to the hole created for the thrusters, in which the grid is very fine around these holes.

Star-CD provides various differencing scheme in the package in order to produce fluid simulation that best describes the problem nature [3]. The upwind-differencing (UD) scheme was chosen over the other schemes such as central-differencing (CD) and self-filtered central differencing (SFCF). The CD scheme is of higher order scheme (second-order accuracy), interpolates linearly on the nearest neighbouring values, and produces less numerical diffusion. It is assumed here that with the tetrahedral cells refinement, UD produces similar simulation results to that of CD discretisation. SFCF blends UD and CD together and thus making it a second-order accurate. However, this scheme was not chosen due to the fact that it has the possibility of generating additional non-linearity. An example of the CD scheme being applied to flow simulation is described in reference [4].

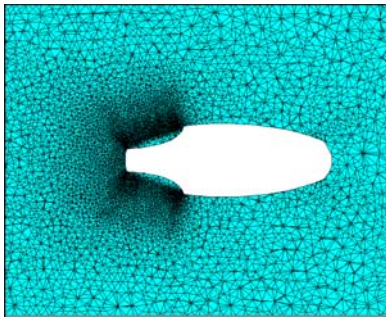


Fig. 3. Grid Refinement around the Holes for the First Model.

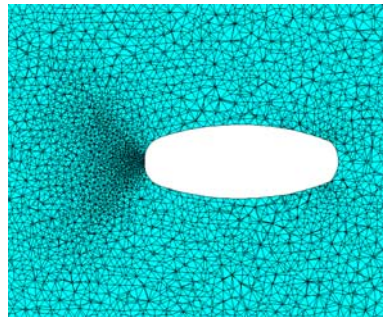


Fig.4. Grid Refinement for the Second Model.

The mass and momentum conservation equations solved by Star-CD for general incompressible and compressible fluid flows (essentially, the Navier-Stokes equations) in Cartesian tensor notation [3], are:

$$\frac{1}{\sqrt{g}} \frac{\partial}{\partial t} (\sqrt{g} \rho) + \frac{\partial}{\partial x_j} (\rho u_j) = s_m \tag{1}$$

$$\frac{1}{\sqrt{g}} \frac{\partial}{\partial t} (\sqrt{g} \rho u_i) + \frac{\partial}{\partial x_j} (\rho u_j u_i - \tau_{ij}) = s_m \tag{2}$$

In the case of laminar flows, Star-CD caters for both Newtonian and non-Newtonian fluids that obey the following constitutive relation, Eq. 3:

$$\tau_{ij} = 2\mu s_{ij} - \frac{2}{3}\mu \frac{\partial u_k}{\partial x_k} \delta_{ij} \quad (3)$$

$$s_{ij} = \frac{1}{2} \left(\frac{\partial u_i}{\partial x_j} + \frac{\partial u_j}{\partial x_i} \right) \quad (4)$$

In the case of turbulent flows, u_i , p and other dependent variables, assuming their ensemble averaged values (equivalent to time averages for steady-state situations) are given for Newtonian fluids:

$$\tau_{ij} = 2\mu s_{ij} - \frac{2}{3}\mu \frac{\partial u_k}{\partial x_k} \delta_{ij} - \overline{\rho u_i' u_j'} \quad (5)$$

where the over bar denotes the ensemble averaging process. The rightmost term in the above represents the additional Reynolds stresses due to turbulent motion. These are linked to the mean velocity field via the turbulence models.

3. Results and Discussion

Two flow cases, a laminar flow model with Reynolds number, $Re = 5 \times 10^5$ and a turbulent flow model with $Re = 3 \times 10^6$ were investigated in this paper. The velocity profile around the submarine is observed according to two different views, (i.e. top or side of the UUV) as shown in Figs. 5 to 7. The pressure profile was also studied and the simulation results showed that the pressure profile is similar in each flow cases for both UUV model.

The character of an external flow field is a function of the shape of the body [5-7]. Flows around relatively simple geometric shapes (e.g. a sphere) are expected to have less complex flow fields than flows past a complex shape such as the UUV. The larger the Reynolds number, the smaller the region of the flow field in which viscous effects are important. This theory was verified in both laminar and turbulent cases as shown in Figs. 5 to 7.

The viscous effect was dominant in the wake region behind the UUV, downstream of the flow direction. The velocity profile is smoother for the second model and the wake is bigger in the case of laminar flow as shown in Figs. 5 and 6.

In the case of turbulent flow, the region ahead of the UUV in which viscous effects are dominant becomes smaller, with the viscous region extending only a short distance upstream of the UUV, Fig. 7. It infers that a smoother velocity profile is obtainable around the hull of the UUV at a higher Reynolds number.

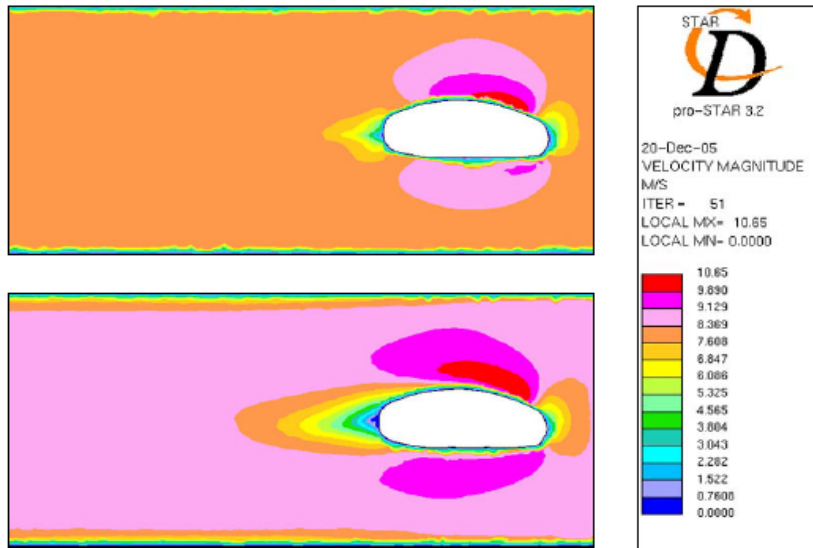


Fig. 5. Velocity Profiles (Side View) for Laminar Flow at Re=500,000 for First Model (top) and Second Model (bottom).

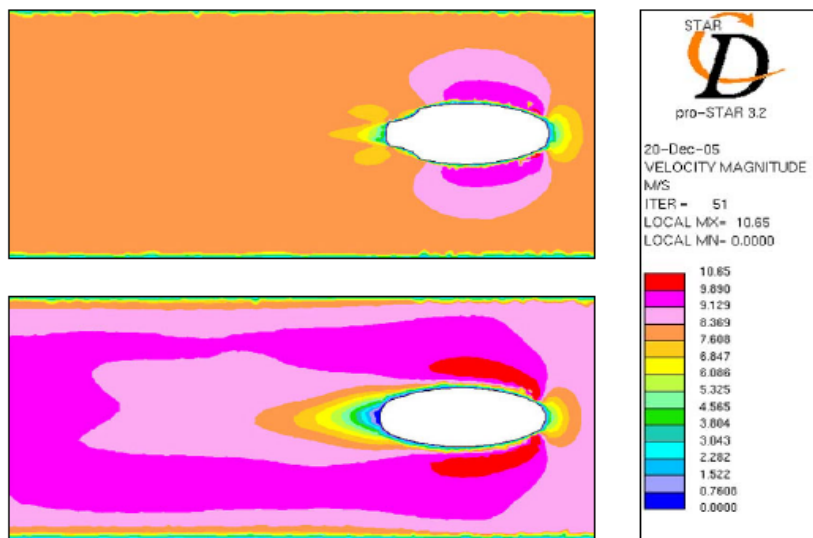


Fig. 6. Velocity Profiles (Top View) for Laminar flow at Re=500,000 for First Model (top) and Second Model (bottom).

A double wake for turbulent flow is also dominant as shown in Fig. 7. A smoother velocity profile for the turbulent flow was also obtained from the second model, with a shorter wakes behind the submarine as shown in Fig. 7.

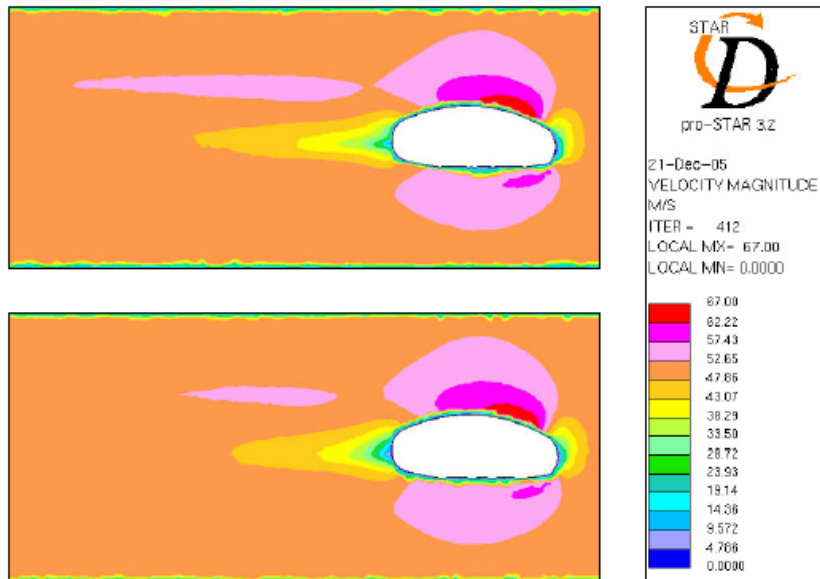


Fig. 7. Velocity Profiles (Top View) for Turbulent Flow at $Re=3,000,000$ for First Model (top) and Second Model (bottom).

4. Conclusions

Two flow cases, a laminar flow with Reynolds number, $Re = 5 \times 10^5$ and a turbulent flow with $Re = 3 \times 10^6$ have been investigated on two UUV models. The larger the Reynolds number, the smaller the region of the flow field in which viscous effects are dominant. The viscous effect was dominant in the wake region behind the UUV, downstream of the flow direction. A smoother velocity profile could be obtained at a high Reynolds number with a smoother velocity profile and a shorter wake for the turbulent flow from the second UUV model.

References

1. Song, F., Edgar, An P., & Folleco, A. (2003) Modelling and Simulation of Autonomous Underwater Vehicles: Design and Implementation. *IEEE Journal of Oceanic Engineering*. 28 (2), 283-296.
2. Baker, C.R., Jeans, T.L., Gerber, A.G., Holloway, A.G.L., & Watt G.D. (2005). Examination of the Flow Separation Characteristics around a Streamlined Axisymmetric Shape. In *Proc. ASME Fluids Engineering Division Summer Meeting and Exhibition*, Houston, Paper No : FEDSM2005-77149, 2005.
3. Computational Dynamics Ltd. (2002). Star-CD Methodology, Star-CD Ver. 3.15A., UK.
4. Mendonça, F., Allen, R., Charentenay, J.D. & Lewis, M. (2002). Towards Understanding LES and DES for Industrial Aero acoustic Predictions. In *Proc. Int. Workshop on 'LES for Acoustics'*, Göttingen, Germany.

5. White, F.M. (2003). *Fluid Mechanics*. (5th ed.). New York: McGraw-Hill.
6. Munson, B.R., Young, D.F. & Okiishi, T.H. (2002). *Fundamentals of Fluid Mechanics*. (4th ed.). John Wiley & Sons.
7. Çengel, Y.A. & Cimbala, J.M. (2005). *Topics in Fluid Mechanics: Fundamentals and Applications*. McGraw-Hill.